Applied Nanoscience (2020) 10:4559–4569
https://doi.org/10.1007/s13204-020-01388-w

ORIGINAL ARTICLE

Thermosensitive hydrogel nanocomposites with magnetic laponite nanoparticles

Olena Goncharuk[1,2] · Yuriy Samchenko[1] · Dariusz Sternik[3] · Lyudmila Kernosenko[1] · Tetyana Poltorats'ka[1] · Natalia Pasmurtseva[1] · Mykola Abramov[2] · Eugen Pakhlov[2] · Anna Derylo-Marczewska[3]

Received: 15 November 2019 / Accepted: 1 April 2020 / Published online: 13 April 2020

Abstract
The thermosensitive nanocomposites based on poly (*N*-isopropylacrylamide) crosslinked by magnetically modified laponite have been synthesized. Using differential scanning calorimetry it was shown that all synthesized hydrogels exhibit a phase transition between the swollen and collapsed states around 32 °C and this temperature depends on the polymer cross-linking method. For hydrogels physically crosslinked by laponite, the phase transition temperature shifts toward higher temperatures compared to the chemically crosslinked hydrogels. The structure of magnetic laponite and composite hydrogels has been characterized by scanning electron microscopy and infrared spectroscopy. The combination of magnetic properties and ability to control the phase transition temperature by changing hydrogel structure suggests that the synthesized hydrogels can be potentially used as a magnetic-driven platform for targeted delivery and drug release or as actuators and elements of microfluidic devices. Thermal destruction of the physically crosslinked hydrogel with incorporated magnetic laponite is observed in the region of 300–400 °C which allows classifying them as relatively heat-resistant materials and can extend existing and open up new application areas for the developed thermosensitive nanocomposites.

Keywords Magnetically modified laponite · Thermosensitive hydrogel · Phase transition · *N*-isopropylacrylamide

Introduction

Materials capable rapidly and predictably to change their physicochemical parameters under the influence of minor changes in the environment are of interest for use as matrices for the controlled release of biologically active substances, especially medicines and drugs (Langer and Tirrell 2004). To this end, nanosized systems for drug delivery based on liposomes, micelles, carbon nanotubes, nanoparticles of metals and metal oxides, and dendrimers are created. (Vlerken and Amiji 2006; Haley and Frenkel 2008). However, the scope of application of these nanoscale carriers is limited owing to their low stability and limited time circulating in the bloodstream system. Therefore, so-called nanogels–nanosized hydrogel particles combining the properties of hydrogels and nanomaterials, have an advantage (Kruti and Swapnil 2016). Similar to hydrogels, they are characterized by increased hydrophilicity, have improved mechanical and diffusion properties which can be predictably regulated by varying the monomer composition and cross-linking degree. Due to nano-dimensionality, the high specific surface area is available for bioconjugation and provides required increased circulation period in the blood and the possibility of passive or active targeting of cancer cells (Asadian-Birjand et al. 2012). Such a combination of properties, as well as the presence of a spatial grid in nanogels to immobilize biomolecules, makes them ideal for use in nanomedicine. The so-called "smart" nanogels (Xianjing et al. 2014) are attracted by researchers, due to their ability to respond to a variety of medically important factors (such as pH (Steinhilber et al. 2013), temperature (Molina et al. 2014), ionic strength, etc.) by changing their volume, refractive index, and hydrophilic-hydrophobic balance (Zha et al. 2011).

✉ Olena Goncharuk
iscgoncharuk@meta.ua

[1] Ovcharenko Institute of Biocolloidal Chemistry of NAS of Ukraine, Kyiv, Ukraine

[2] Chuiko Institute of Surface Chemistry of NAS of Ukraine, Kyiv, Ukraine

[3] Chemistry Department, Maria Curie-Sklodowska University, Lublin, Poland

In recent years thermosensitive hydrogels based on of *N*-isopropylacrylamide (NIPAA), which at room temperature are in an expanded hydrated conformation, and when heated—they get into a compact dehydrated state, have been investigated (Molina et al. 2014). The phase transition between the swollen and collapsed states as the temperature increases is caused by increased hydrophobic interactions between isopropyl groups and the destruction of hydrogen bonds with water molecules (Zha et al. 2011). The phase transition temperature of such hydrogels is close to 32 °C, which approaches the temperature of the human body and can be shifted to higher or lower temperatures after NIPAA copolymerization with hydrophilic or hydrophobic monomers (Shah and Patel 2014), respectively, which allows using these materials to create temperature-controlled drug delivery systems. Such hydrogels can be easily synthesized and characterized by a clear phase transition at 32 °C, but at the same time they have some significant drawbacks that limit their application: first of all, increase in opaqueness with an increasing the crosslinking degree and low mechanical strength and elasticity (Gao et al. 2013). In addition, they have predominantly low equilibrium water content and a slow response rate to changes in their environment, in particular, the rate of transition to a collapsed state (Samchenko et al. 2015). These deficiencies can be addressed by modifying the hydrogel synthesis method (Haraguchi et al. 2002) and utilizing the physical crosslinking of copolymer with nanoparticles of laponite (synthetic clay, analogue of natural hectorite) instead of chemical crosslinking with bifunctional monomers. In recent years, due to the unique and homogeneous three-dimensional structure of the laponite nanocomposite hydrogels caused by the strong negative charge of the laponite disks and the weak positive charge of the ribs (Liu et al. 2006), they have been extensively investigated in relation to their improved mechanical properties (Xiong et al. 2008), potential biological applications (Kokabi et al. 2007), improved responses to stimuli (Wang and Chen 2012), and so on. Nanocomposites based on laponite and various acrylic monomers, in particular, acrylamide (Okay and Oppermann 2007), acrylic acid (Huili et al. 2014), NIPAA (Shibayama et al. 2004; Korotych et al. 2013), dimethylacrylamide (Haraguchi et al. 2003), etc. were synthesized and investigated.

The efficiency of drug release and the targeting of delivery can be greatly improved by providing drug carriers with magnetic properties (Manilo et al. 2015) since chemotherapeutic agents attached to magnetosensitive nanocomposites can be concentrated in the immediate proximity to the target organ by imposing an external magnetic field. At the same time, by imposing a low-intensity alternating magnetic field, it is possible to achieve contactless heating of a thermosensitive hydrogel nanocomposite with an incorporated magnetic laponite owing to its oscillation and, as a consequence, a transition to a collapsed state with spontaneous release of incorporated medicines.

This work is devoted to the synthesis and study of the physicochemical properties of thermosensitive nanocomposites based on NIPAA crosslinked by magnetically modified laponite.

Materials and methods

Synthesis of magnetically modified laponite (MLAP), the schematic diagram of which is shown in Fig. 1, was performed as follows: 3 g of laponite (Laponite RD, Rockwood Additive Limited, 99%, specific surface 370 m^2/g, density 1000 kg/m^3, chemical composition: SiO_2 59.5%, MgO 27.5%, Li_2O 0.8%, Na_2O 2.8%) was stirred in 200 mL of distilled water in a magnetic stirrer at room temperature, and then dispersed in an ultrasonic bath for 10 min. Then the laponite dispersion was heated to 70 °C. Separately, a solution of 2.43 g of $FeSO_4 \cdot 7H_2O$ and 2.66 g of $FeCl_3$ with Fe^{3+}:Fe^{2+} molar ratio of 2:1 in distillated H_2O (20 mL) was prepared, after which laponite was quickly added to the solution and mixed for 10 min in a nitrogen atmosphere. The pH was adjusted to 10 by adding slowly concentrated ammonia hydroxide and continuous stirring for 2 h at 70 °C (Ali et al. 2016; Fu and Ravindra 2012). The formed black precipitate Fe_3O_4 was concentrated with a magnet and rinsed with distilled water to pH 7.

As it is known, nanodiscs (particles) of laponite consist of an octahedral layer which is surrounded by two silicate tetrahedral layers. The molecular formula of laponite has the following form—$Na^+_{0.7}[(Si_8Mg_{5.5}Li_{0.4})O_{20}(OH)_4]^-_{0.7}$. In an aqueous solution, laponite particles, which are charged negatively, can electrostatically bind to stacks with sodium counterions (Haraguchi et al. 2003).

Synthesis of thermosensitive hydrogels (Fig. 2) based on the NIPAA (Sigma-Aldrich, 97%), cross-linked using MLAP (or LAP) was performed as follows: 0.3 g of MLAP (or LAP) and 0.6 g of NIPAA were dispersed in an ultrasonic bath for 1 min in 4 mL of 4% aqueous $Na_4P_2O_7$ solution. The components of the oxidation–reduction initiating system were added: ammonium persulfate, PSA (Sigma, 98%) and *N,N,N′,N′*-tetramethylethylenediamine, TMED (Merck, ≥ 99%), purged with argon for 3 min, and poured

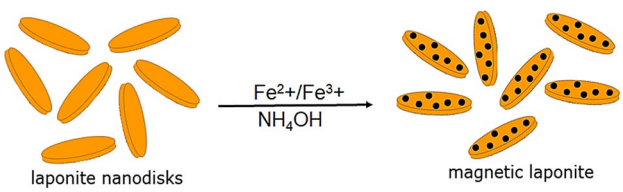

Fig. 1 Scheme of MLAP synthesis

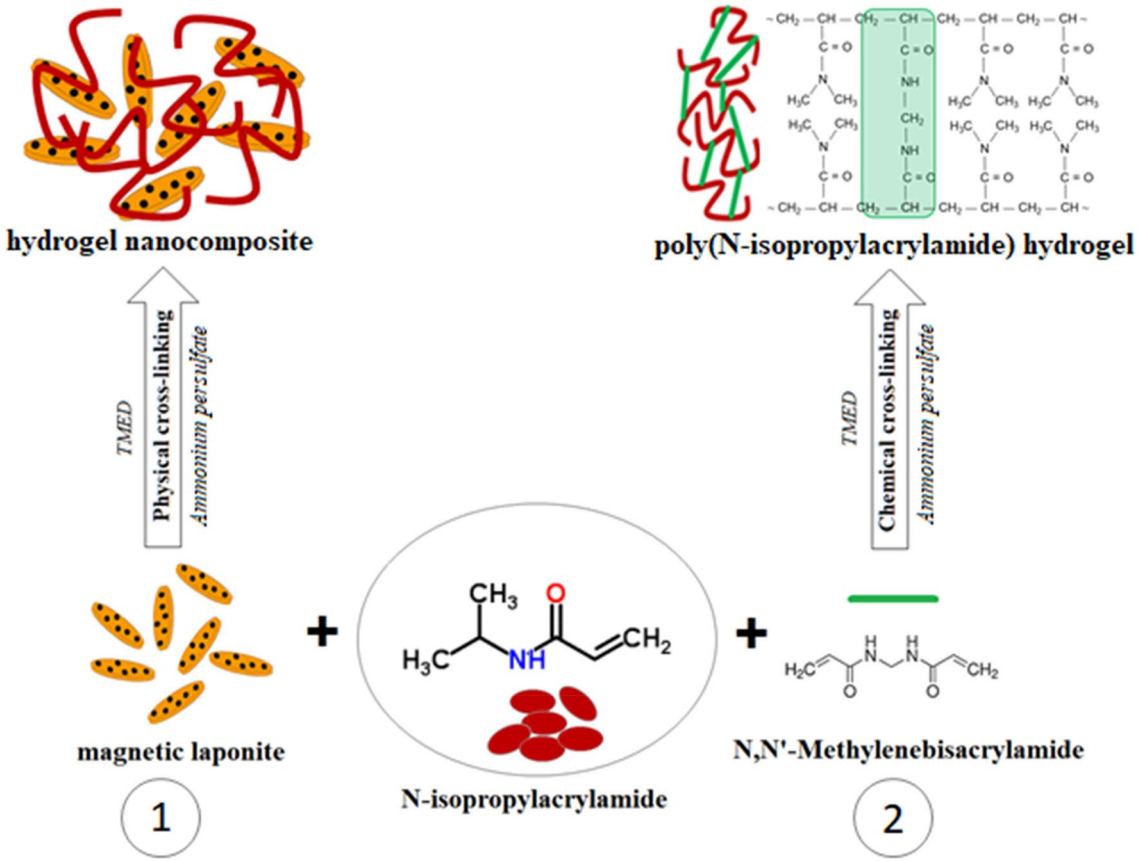

Fig. 2 Scheme of the structure of chemically and physically crosslinked hydrogels

between two glass plates separated by spacers with the thickness of 0.7 mm. Chemically crosslinked hydrogel was synthesized in the following way: 0.6 g NIPAA were dispersed in an ultrasonic bath for 1 min in 4 mL of water, then 0.3 mL of a 3% *N,N'*-methylene-*bis*-acrylamide (MBA) solution was added under stirring, and the mixing was continued for 15 min. The components of the oxidation–reduction initiating system (PSA and TMED) were added, purged with argon for 3 min, and poured between two glass plates separated by spacers with the thickness of 0.7 mm.

Investigation of MLAP magnetic properties

The hysteresis loops of the magnetic moment of the samples were measured using a laboratory vibrating Foner's type magnetometer at room temperature. Measuring equipment description and measurement method are outlined in the previously published work (Borysenko et al. 2007). The MLAP nanocomposite distributed with a volumetric concentration ~ 0.05 in a bulk paraffin matrix to prevent dipole–dipole interaction was used for measurements. Materials with known values of the specific saturation magnetization (σ_s): tested sample of nickel and nanoparticles of Fe_3O_4 (98%) produced by "Nanostructured & Amorphous Materials Inc.", USA were used for comparison. The measurement uncertainty in σ_s relative to the reference samples was below 2.5%.

The size distribution of the MLAP in the colloid was found by magnetic granulometry (Bean and Jacobs 1956), which is based on a comparison of the experimental magnetization curve with the Langevin function for given laws of particle size distribution and their magnetic parameters, in particular, the saturation magnetization of the particle material and the thickness of the demagnetized layer, according to the magnetization curve (MC). To analyze the MCs the well-known Eq. (1) was used (Kaiser and Miscolezy 1970):

$$\sigma(H) = \sigma_s^b \frac{\sum_{i=1}^{k} p_i(d)(d_i - 2a_0)^3 L\left(\frac{\rho\sigma_s^b H}{k_B T}\frac{\pi}{6}(d_i - 2a_0)^3\right)}{\sum_{i=1}^{k} p_i(d) d_i^3}, \quad (1)$$

where $p(d) = \frac{1}{d\sigma_{\ln d}\sqrt{2\pi}} \exp\left\{\frac{-(\ln d - \mathrm{M}[\ln d])^2}{2\sigma_{\ln d}^2}\right\} d_i$ and n_i—diameter and number of magnetite particles in *i*-fractions, respectively, determined from the histogram; a_0—non-magnetic layer thickness; $L(\xi) \equiv cth\xi - 1/\xi$—the Langevin function.

Scanning electron microscopy (SEM)

The surface morphology of composites was analyzed using field emission scanning electron microscope QuantaTM 3D FEG (FEI, USA) operating at the voltage of 30 kV.

Infrared (IR) spectroscopy

A mixture of dried xerogel or MLAP with dry KBr at 1:100 mass ratio was grinded and pressed into thin transparent plates at a pressure of 99 MPa. IR spectra of KBr pelleted samples were recorded over the 4000–400 cm^{-1} range using a Specord M80 IR spectrometer in the transmission mode with a step of 4 cm^{-1} and an integration time of 1 s. The obtained transmission data were transformed to absorbance with the help of a computed polynomial "best fit" baseline for the original spectrum.

Thermal analysis

Thermal analysis was carried out using a STA 449 Jupiter F1 (Netzsch, Germany) apparatus on ~ 16 mg of the sample placed into a corundum crucible with an airflow of 50 mL·min^{-1}, a heating rate of 10 °C min^{-1}, and S TG-DSC sensor thermocouple type. For studies of thermal decomposition of dry hydrogels, DSC was carried out in the temperature range of 30–950 °C, and to study the phase transitions of water in the swollen hydrogels—the DSC was carried out in the temperature range from –50 to + 60 °C. Empty corundum crucible was used as a reference. The gaseous products emitted during decomposition of the materials were analyzed by a FTIR Brucker (Germany) spectrometer and QMS 403DAëolos (Germany) coupling on-line to STA instrument. The QMS data were gathered in the range from 10 to 200 Da. The FTIR spectra were recorded in the range of 4000–600 cm^{-1} with 16 scans per spectrum at a resolution of 4 cm^{-1}.

Investigation of hydrogel swelling

Swelling degree Q of hydrogels at different temperatures in grams of an absorbed solvent per gram of a dry polymer was determined gravimetrically according to the formula:

$$Q = \left(m_{sw} - m_{dry}\right)/m_{dry} \quad (2)$$

where m_{sw} and m_{dry} are masses of the swollen (mass of an equilibrated hydrogel after 24 h in distillate water) and dry xerogel, respectively, [g].

Results and discussion

Magnetic properties of MLAP

The hysteresis loops of the magnetic moment of the MLAP sample are shown in Fig. 3a. It can be seen from them that the synthesized MLAP sample is characterized by a small area of the hysteresis loop, i.e., low coercive force; namely, it is characterized by values of coercive force H_c 37 Oe and specific saturation magnetization σ_s 33.2 G•cm^3/g. The specific magnetization of the saturation σ_s of the samples was found from the dependence $\sigma(H)$ at $H \to \infty$. It has a lower value than the corresponding characteristics of bulk crystals (Shliomis 1974) and in the range of characteristic values for nanoscale materials.

In the general case, a macroscopic ferro- or ferrimagnetic particle has a domain structure, the process of its

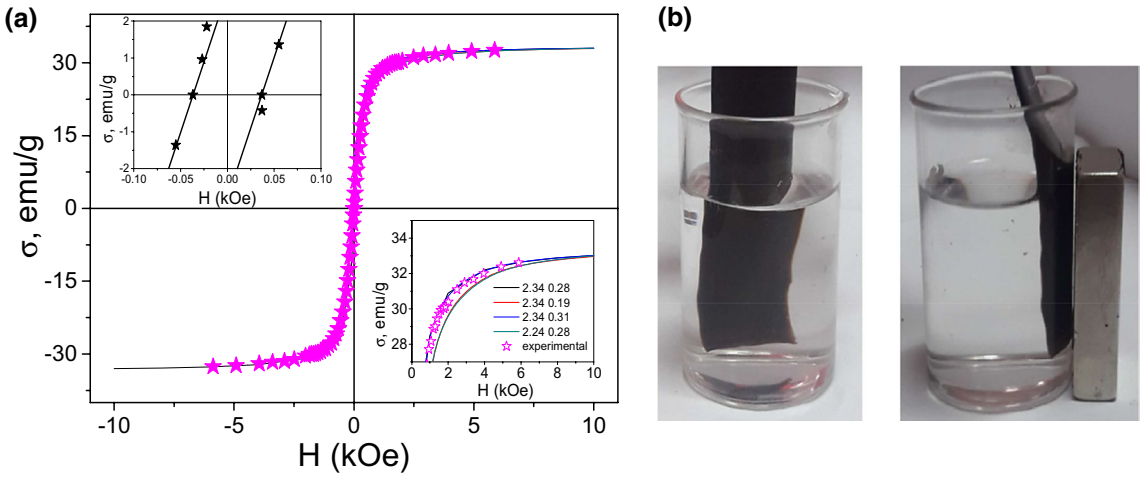

Fig. 3 Hysteresis loop of specific saturation magnetization and fitting of Eq. (1) to the experimental MCs of MLAP nanocomposite (**a**) and interaction the hydrogel crosslinked by MLAP with a magnet (**b**)

magnetization reversal occurs mainly through the displacement of domain walls, which leads to low values of *Hc*. As the particle size decreases a single-domain state is realized, which is characterized by maximum H_c, since magnetization reversal is carried out by rotating the particle. For each ferro- and ferrimagnetic material there is a critical size below which its particles become single-domain. Single domain critical size (d_{cr}) and the corresponding H_c determined experimentally for ferrimagnetic Fe_3O_4 are ≥ 50 nm and 375–440 Oe, respectively, at room temperature (Kirschvink et al. 1985). With a further reduction of the particle size to a value corresponding to the superparamagnetic limit (d_{sup}), H_c decreases rapidly to zero due to the increasing role of thermal fluctuations. A particle of diameter (D) under the condition $d_{sup} < D < d_{cr}$ is in a blocked ferrimagnetic state and under the condition $d_f < D \leq d_{sup}$ (d_f is the ferromagnetic limit) is in a superparamagnetic state. The ensemble of particles in the superparamagnetic state has a hysteresis-free magnetization reversal curve and, therefore, zero values of H_c and remnant magnetization (M_r). The particle with $D \leq d_f$ loses its ferromagnetic properties.

The magnetic technique for particle size estimation or magnetic granulometry is based on the matching of a modeling Langevin curve with the experimental MC for a corresponding system of ferromagnetic particles. The average magnetic moment per particle is obtained from this analysis, and the average particle size is thus determined. By fitting the $\sigma(H)$ curve data points to an integral over the size distribution and the Langevin function, the mean diameter and the standard deviation (RMS) of the size distribution can be extracted (Eberbeck et al. 2011). The size distributions of the investigated MLAP nanoparticles were estimated by fitting Eq. 1 to the MCs (Fig. 3b). The results are listed in Table 1 and Fig. 4.

Characterization of the composite structure

As the SEM images reveal (Fig. 5a, b), the layered configuration of initial laponite is noticeable, the elementary

Table 1 Statistical parameters of ensembles of Fe_3O_4 nanoparticles

Sample	M[d], nm	σ_d, nm	M[ln d]	$\sigma_{\ln d}$
NPFe_3O_4+	10.6		2.34	0.19
NPFe_3O_4+	10.8	2.93	2.34	0.28
NPFe_3O_4+	10.9		2.34	0.31
NPFe_3O_4+	9.77		2.24	0.28
NPFe_3O_4+	8.84		2.14	0.28

M[d], M[ln d]—mathematical expectation of diameter and logarithm of diameter, respectively; σ_d and $\sigma_{\ln d}$ are the RMS of the diameter and the logarithm of the diameter, respectively

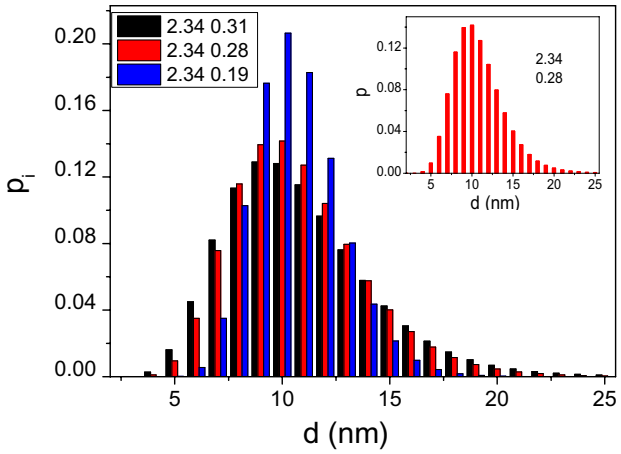

Fig. 4 Size distribution of synthesized MLAP nanoparticles obtained from magnetic particle size analysis of MCs

primary particle of which has an anisotropic structure (length about 25 nm and wall thickness of 1 nm) with the ability to form stack aggregates. Thus, in Fig. 5 primary particles of 20–30 nm in size are observed, the aggregation of which occurs in two directions, as a result of which (Fig. 5a) the thickness of the layers somewhat increases.

As a result of the intercalation of magnetite into the crystalline lattice of initial laponite, the structure of the composite material varies considerably. In SEM-image of the magnetic laponite composite (Fig. 5c, d), layered aggregates characteristic of the initial laponite are not observed, but spherical particles 5–10 nm in size available that can be attributed to the formed structure of magnetite. The structure of the synthesized laponite-magnetic composite is rather homogeneous, with a narrow particle size distribution. Since the use of laponite as a substrate for the formation of the magnetite structure, including the nucleation and growth of crystals, is spatially limited to the distance between the layers of the initial laponite and, to some extent, is determined by the cation exchange capacity of the laponite, it can be confirmed that such conditions provide the formation of exclusively nanosized particles of magnetite.

There are characteristic absorption bands in the IR spectrum of the initial laponite (Fig. 6), namely, the peak at 3645 cm^{-1} which corresponds to stretching vibrations of nonhydrogen-bonded or "free" surface hydroxyl groups and a broadband centered around ~ 3400 cm^{-1} corresponding to the O–H oscillations of physically adsorbed water and hydroxyl groups that formed hydrogen bonds with water molecules and other hydroxyl groups. A peak at 1628–1636 cm^{-1} corresponds to the deformation oscillations of adsorbed water. This band is also observed in the spectrum of hydrogel filled with magnetic laponite. Strong band in the area of 1000 cm^{-1} can be assigned to the asymmetric oscillations of the Si–O bonds in layered silicates and it is

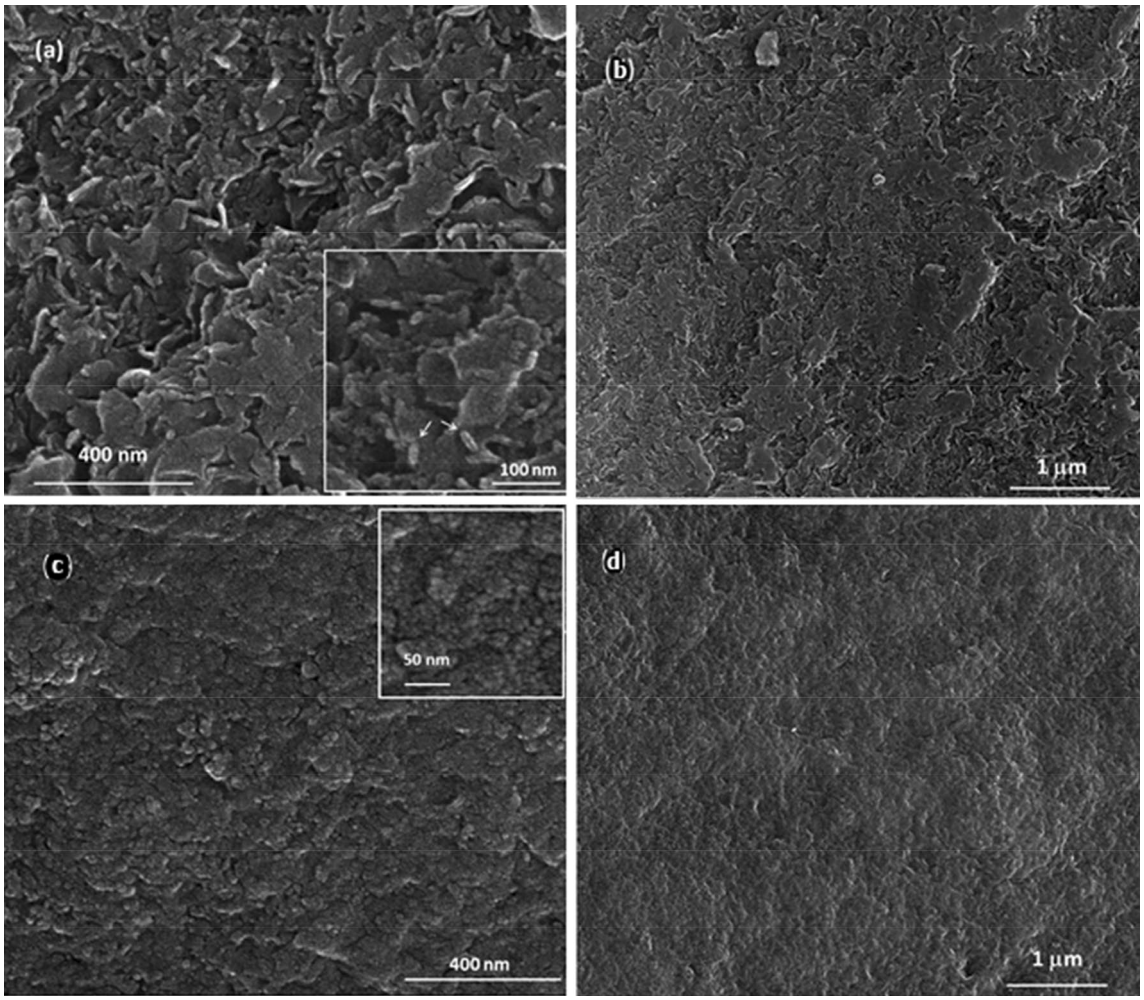

Fig. 5 SEM image of the unmodified laponite (**a** and **b**) and MLAP composite (**c** and **d**)

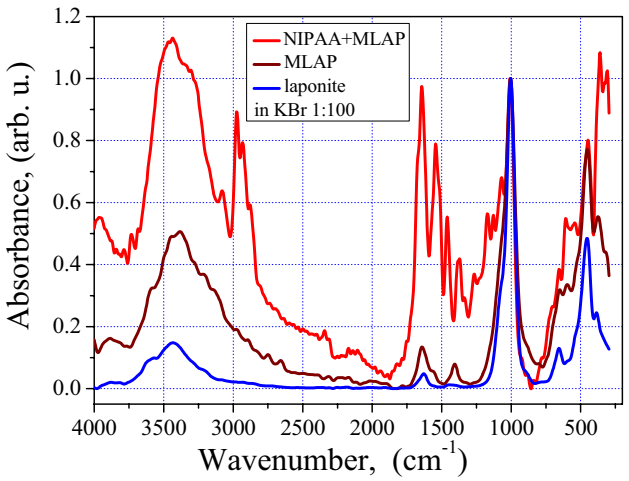

Fig. 6 IR spectra of unmodified laponite, MLAP, and poly(NIPAA) hydrogel crosslinked by MLAP normalized to the band at 1008 cm^{-1}

observed in both the spectrum of the pristine laponite and in the spectra of the laponite/magnetite composite and hydrogel nanocomposite. In the spectrum of a hydrogel nanocomposite the bands at 1559 cm^{-1} corresponding to the deformation oscillations of the N–H bond, at 1628 cm^{-1}—corresponding to the carbonyl group oscillations, as well as two typical peaks at 1372 and 1391 cm^{-1}, corresponding to the C–H fluctuations of the group $–CH(CH_3)_2$ are observed.

Thermal analysis of dried hydrogels

The thermal characteristics (TG, DTG, and DSC) of dried hydrogel filled with magnetic laponite were studied upon heating of samples in helium atmosphere (Fig. 7).

In the case of thermal decomposition of dried hydrogels (Fig. 7) the weight losses are results of the process of desorption of physically adsorbed water and dehydroxylation in the temperature range up to 720 °C, and removing of

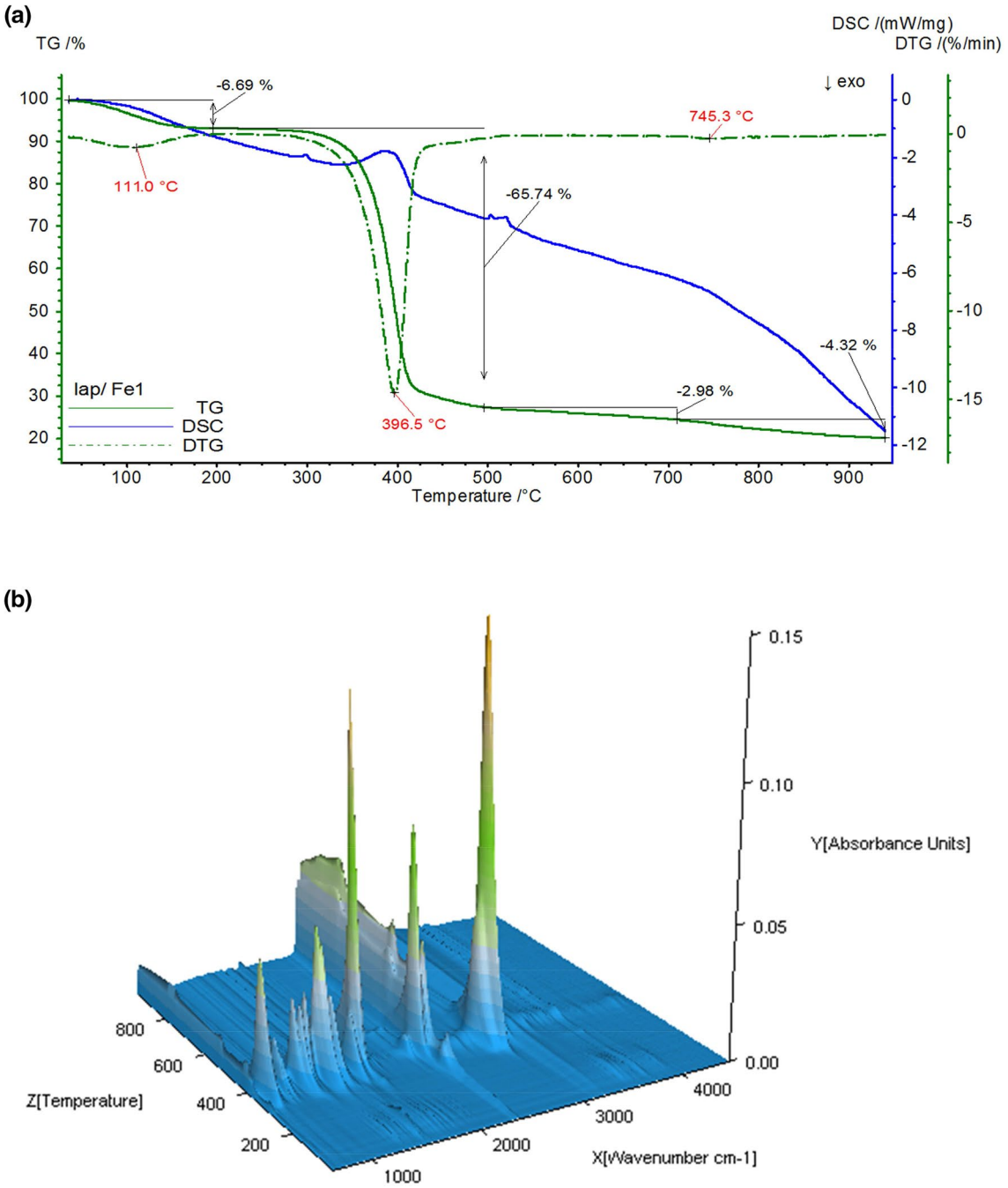

Fig. 7 DTG, TG, and DSC curves (**a**) and FTIR-TG space image of thermal degradation products of the gel (**b**) in a helium atmosphere for dried hydrogel filled with MLAP

carbonates at higher temperatures. According to the literature (Yariv 2004; He et al. 2006; Majdan et al. 2006) the thermal decomposition of organic molecules is very complicated and occurs in a few main stages.

The first stage comprises physicochemical transformation (dehydration, melting, changes in the conformation of molecules, initial defragmentation, etc.) and occurs at low temperature. The processes of defragmentation and partial oxidation of the H atoms prevail mainly in the temperature range up to 400 °C. At the temperatures above 500 °C the peaks on DTG or DSC curves are attributed to processes of thermo-oxidation of H and N atoms and pyrolysis producing a solid carbon residue and volatile products. According to the IR spectra of the emitted volatile products (Fig. 7b), the composition of gas mixture mainly contains CO_2 (bending oscillation at 660 cm^{-1} and stretching

oscillations at 2283 cm^{-1} and 2343 cm^{-1}), H_2O (3280 cm^{-1} and 1660 cm^{-1}), and nitriles (2250 cm^{-1} C≡N stretching and 2950 cm^{-1} C–H stretching), which is consistent with published data (Schild 1996; Carrillo et al. 2009).

The low-temperature mass loss from 30 to 150 °C for hydrogels corresponds to physically sorbed water desorption. The main weight loss was found for the polymer degradation stage (300–450 °C). This stage of polymer molecules decomposition was confirmed by the increasing peaks for water and carbon dioxide in the IR spectra (Fig. 7b) of thermal degradation products of the analyzed samples.

Temperature effect on swelling of NIPAA hydrogels

As it was mentioned above, hydrogels based on poly(NIPAA) show a volume phase transition around 32 °C. At higher temperatures, poly(NIPAA) hydrogels shrink and expel water from gel networks. This process is reversible, and at lower temperatures the interaction between water and polymer chains becomes favorable, and the hydrogels swell back after absorbing water. The use of initial or magnetic laponite for crosslinking of NIPAA chains leads to significant changes in the structure compared to the chemically cross-linked hydrogel and can result in the swelling process changes. The influence of the hydrogel compositions on the swelling behavior of thermosensitive NIPAA-based hydrogels was studied in the temperature range from 25 °C, which is lower than the phase transition temperature, to 45 °C, which is above the phase transition temperature. As it can be seen in Fig. 8, the largest swelling degree at room temperature is observed for the hydrogel sample with incorporated magnetic laponite, following by laponite-containing hydrogel composite, and finally chemically cross-linked hydrogel. In general, the swelling degree is affected by balance between hydrophilicity and hydrophobicity of copolymer units and the crosslinking density of the network. Because of a relatively low crosslinking density the hybrid NIPAA-based hydrogels with magnetic laponite show a high swelling capacity reaching the swelling degree ~ 28.2 g/g while keeping relatively good mechanical properties. The degree of swelling for samples with magnetic laponite is almost twice as high as for chemically crosslinked poly(NIPAA), but at the same time, the modification of NIPAA-based hydrogel with initial (not magnetic) laponite affects the degree of swelling slightly. It should be noted that the equilibrium swelling degree of all samples at temperatures above the phase transition decreases to 0.13–0.42 g/g. Dynamics of water loss for all samples is similar.

More detailed information on the thermally triggered phase transition can be given by the DSC analysis. Essentially, the phase transition of the thermosensitive hydrogel,

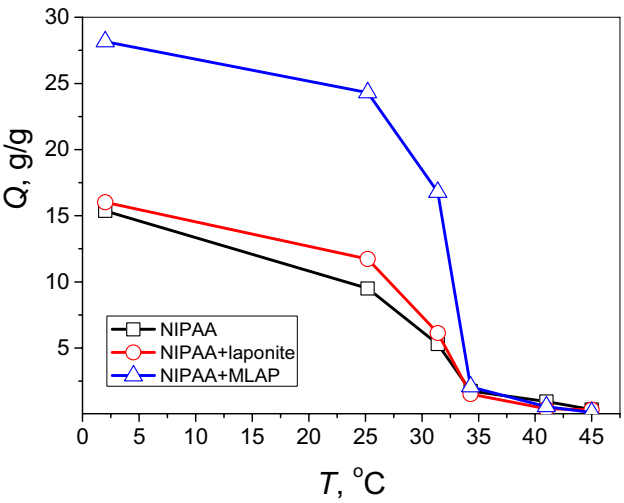

Fig. 8 Temperature dependence of the swelling degree of NIPAA-based hydrogels of different composition

occurring with the change of the environmental temperature, is a phase separation process; therefore, it is accompanied with a special critical heat of phase transition at so-called lower critical solution temperature (LCST) (Aixiang et al. 2007; Teotia et al. 2015; Klouda and Mikos 2008). Figure 9a–d shows the DSC thermograms of NIPAA-based hydrogels: chemically crosslinked and filled with the initial and magnetic laponite. The temperature of the onset of the phase transition shifts towards higher temperatures for poly(NIPAA) gel modified with laponite and magnetic laponite compared with chemically crosslinked NIPAA-based gel.

The maximum phase transition shift is observed for hydrogel modified with initial laponite with phase transition onset at 34.2 °C unlike the chemically cross-linked NIPAA-based hydrogel, for which the start of the phase transition is observed at 31.8 °C and corresponds to the literature data (Aixiang et al. 2007). The onset of the phase transition for hydrogels modified with magnetic laponite occurs at 34.0 °C. NIPAA-based hydrogels filled with unmodified or magnetically modified laponite show a maximum of LCST around 36.4 and 35.2 °C, respectively (Fig. 9b–c). For the unfilled poly(NIPAA) gel the maximum of LCST is around 34.7 °C (Fig. 9a), i.e., a slight shift towards higher temperatures is observed for a gel filled with magnetic laponite. The DSC curve for a hydrogel filled with unmodified laponite shown in Fig. 9b indicates the influence of laponite as a crosslinking agent on the structure and temperature-sensitive properties of NIPAA-based hydrogels: in the presence of laponite the LCST is shifted to higher temperatures compared to a chemically crosslinked NIPAA hydrogel.

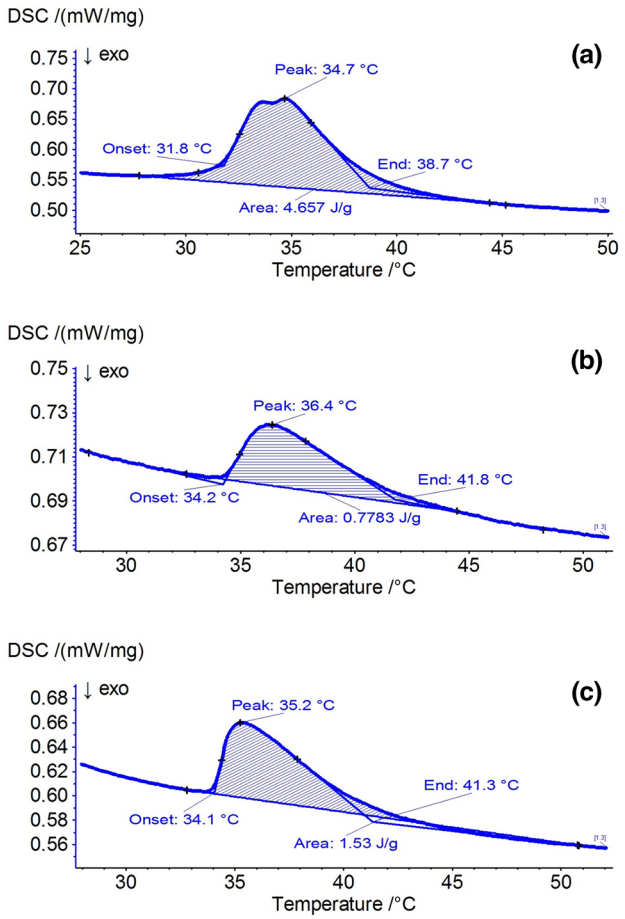

Fig. 9 DSC curves of NIPAA-based hydrogels around LCST: chemically cross-linked (**a**); physically cross-linked with unmodified laponite (**b**); and physically cross-linked with MLAP (**c**)

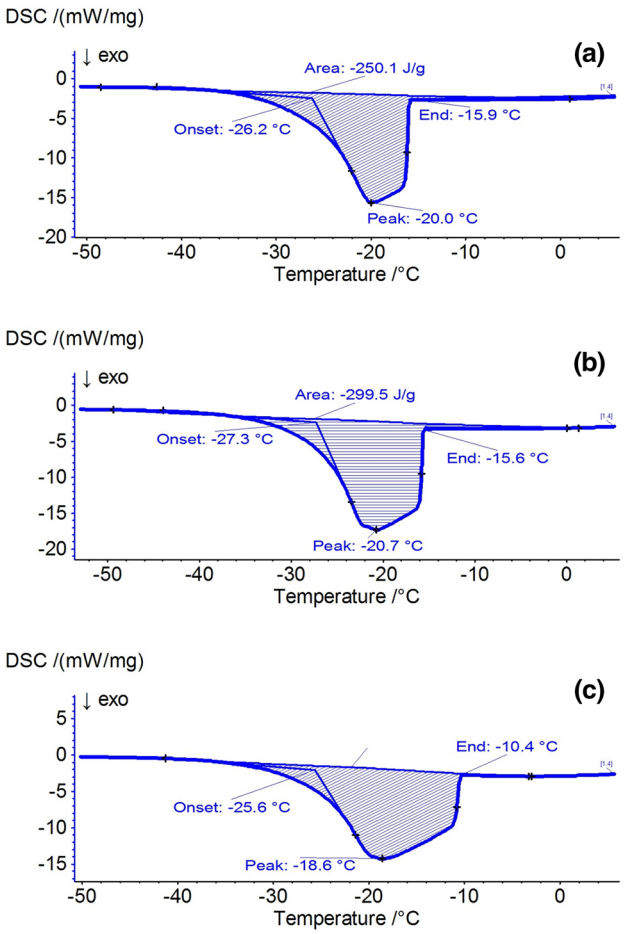

Fig. 10 DSC curves of NIPAA hydrogels upon freezing: chemically cross-linked (**a**); physically cross-linked with unmodified laponite (**b**); and physically cross-linked with MLAP (**c**)

Investigation of water freezing and melting in hydrogels

Figures 10 and 11 show the DSC heating thermograms obtained for NIPAA-based hydrogels. Ice melting–freezing occurs at different temperatures, depending on the water sample size: the smaller the volume, the lower the freezing temperature is observed for small clusters of water (Dalmazzone and Noïk 2009). The complete process of crystallization is very fast, therefore, a significant amount of energy is released in a very short time, so, the first part of the exothermic freezing peak is sharp (Fig. 10). The nucleation is a stochastic phenomenon; therefore, the freezing temperature is expected to vary for different samples. The peak maximum of water freezing is observed in the range from − 18.6 to − 20.7 °C for all three studied hydrogels. On the contrary, whatever the sample size, the beginning of ice melting is observed at 0 °C with a melting peak being broader than a freezing peak. The DSC data show a broad sharp endothermic peak associated with the melting of the solid phase of water (Fig. 11). The melting peak is broad and can be decomposed to the melting of different phases of water. There were distinguished melting peaks with maximum values in the temperature range from + 7.2 to + 9.4 °C.

Conclusions

Thermosensitive hydrogels based on NIPAA have been synthesized by methods of chemical crosslinking and physical crosslinking with of unmodified and magnetically modified laponite. The synthesized MLAP composite and NIPAA-based hydrogel with incorporated MLAP have demonstrated distinct magnetic responsiveness. The investigation of magnetic properties showed that MLAP composite pertain to soft magnetic materials with a small area of the hysteresis loop and value of coercive force *Hc* equals 37 Oe and specific saturation magnetization σ_s equals 3.2 G•cm^3/g. These characteristics allow the poly(NIPAA) hydrogel with incorporated MLAP to be

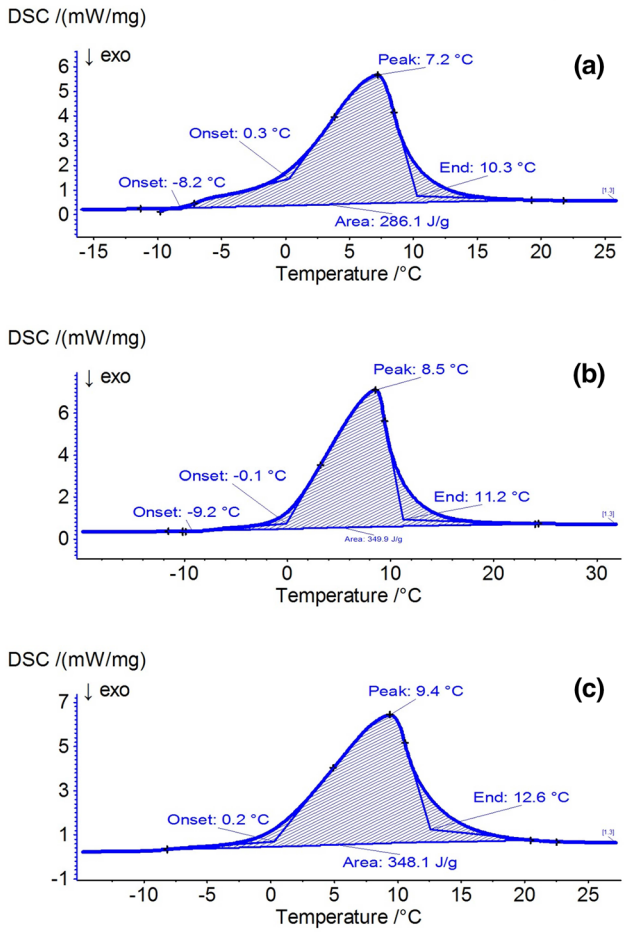

Fig. 11 DSC curves of NIPAA hydrogels upon melting: chemically cross-linked (**a**); physically cross-linked with unmodified laponite (**b**); and physically cross-linked with MLAP (**c**)

used for targeted contactless drug delivery under application of weak magnetic fields. The average particle size of magnetite in the MLAP composite, estimated by magnetic granulometry and SEM methods, was 10.9 nm, which indicates its attribution to nanoscale fillers. Utilizing DSC, the thermal properties of swollen hydrogels were investigated in the temperature range corresponding to phase transition during swelling/deswelling around 32 °C (lower critical solution temperature), and also in the range of temperature of water freezing and melting. Dried xerogels were investigated in the temperature range corresponding to their thermal decomposition. It was found that the synthesis method affects the swelling processes of the synthesized hydrogels, namely, for a hydrogel physically crosslinked with magnetic laponite, the swelling degree is higher, and LCST shifts towards higher temperatures compared to the chemically cross-linked hydrogel. Thermal destruction of the hydrogels physically crosslinked by a magnetic laponite is observed in the region of 300–400 °C, which makes it possible to classify them as relatively heat-resistant materials which allows classifying them as relatively heat-resistant materials and can extend existing and open up new application areas for the developed thermosensitive nanocomposites.

Compliance with ethical standards

Conflict of interest On behalf of all authors, the corresponding author states that there is no conflict of interest.

References

Aixiang Q, Mangeng L, Qunfeng L, Ping Z (2007) Synthesis and characterization of thermo-sensitive poly(*N*-isopropylacrylamide) hydrogel with fast response rate. Front Chem China 2:135–139. https://doi.org/10.1007/s1145800700282

Ali A, Zafar H, Zia M, ul Haq I, Phull AR, Ali JS, Hussain A (2016) Synthesis, characterization, applications, and challenges of iron oxide nanoparticles. Nanotechnol Sci Appl 9:49–67. https://doi.org/10.2147/nsa.S99986

Asadian-Birjand M, Sousa-Herves A, Steinhilber D, Cuggino JC, Calderon M (2012) Functional nanogels for biomedical applications. Curr Med Chem 19:5029–5043

Bean CP, Jacobs IS (1956) Magnetic granulometry and super-paramagnetism. J Appl Phys 27:1448–1452

Borysenko NV, Dubrovin IV, Abramov NV, Bogatyriov VM, Gayevaya MV, Gorbik PP (2007) Synthesis and properties of magnetically sensitive nanocomposites based on iron and silicon oxides. In: Shpak AP, Gorbik PP (eds) Physical chemistry of nanomaterials and supramolecular structures. Naukova dumka, Kyiv, pp 394–406 **[in Russian]**

Carrillo F, Defays B, Colom X, Sunol JJ, Lopez-Mesas M (2009) Thermal degradation of lyocell/poly-*N*-isopropylacrylamide graft copolymers gels. J Therm Anal Calorim 97:945–948

Dalmazzone C, Noïk C, Clausse D (2009) Application of DSC for emulsified system characterization. Oil Gas Sci Technol 64:543–555. https://doi.org/10.2516/ogst:2008041

Eberbeck D, Wiekhorst F, Wagner S, Trahms L (2011) How the size distribution of magnetic nanoparticles determines their magnetic particle imaging performance. Appl Phys Lett 98:182502

Fu Ch, Ravindra NM (2012) Magnetic iron oxide nanoparticles: synthesis and applications. Bioinspir Biomim Nanobiomater 1:229–244. https://doi.org/10.1680/bbn.12.00014

Gao H, Wang N, Hu X (2013) Double hydrogen-bonding pH-sensitive hydrogels retaining high-strengths over a wide pH range. Macromol Rapid Commun 34:63–68. https://doi.org/10.1002/marc.201200548

Haley B, Frenkel E (2008) Nanoparticles for drug delivery in cancer treatment. Urol Oncol 26:57–64

Haraguchi K, Takehisa T, Fan S (2002) Effects of clay content on the properties of nanocomposite hydrogels composed of poly(NIPAA) and clay. Macromolecules 35:10162–10171

Haraguchi K, Farnworth R, Ohbayashi A, Takehisa T (2003) Compositional effects on mechanical properties of nanocomposite hydrogels composed of poly(*N*, *N*-dimethylacrylamide) and clay. Macromolecules 36:5732–5741

He H, Frost RL, Bostrom T, Yuan P, Duong L, Yang D, Xi Y, Kloprogge JT (2006) Changes in the morphology of organoclays with HDTMA+ surfactant loading. Appl Clay Sci 31:262–271

Huili L, Renbao G, Shimei X (2014) Surfactant-assisted synthesis of a transparent ionic nanocomposite hydrogel. Appl Clay Sci 101:335–338

Kaiser R, Miscolezy G (1970) Magnetic properties of stable dispersions of subdomain magnetic particles. J Appl Phys 1:1064–1072

Kirschvink JL, Jones DS, MacFadden BJ (eds) (1985) Magnetite biomineralization and magnetoreception in organisms: a new biomagnetism. Plenum Press, New York/London

Klouda L, Mikos AG (2008) Thermoresponsive hydrogels in biomedical applications—a review. Eur J Pharm Biopharm 68:34–45. https://doi.org/10.1016/j.ejpb.2007.02.025

Kokabi M, Sirousazar M, Hassan ZM (2007) PVA–clay nanocomposite hydrogels for wound dressing. Eur Polym J 43:773–781

Korotych O, Samchenko Yu, Boldesku I, Ulberg Z, Zholobak N, Sukhodub L (2013) N-isopropylacrylamide-based fine dispersed thermosensitive ferrogels obtained via in-situ technique. Mater Sci Eng 33:892–900

Kruti SS, Swapnil S (2016) Nanogels: an overview of properties, biomedical applications and obstacles to clinical translation. J Control Release 240:109–126

Langer R, Tirrell D (2004) Designing materials for biology and medicine. Nature 428:487–492

Liu Y, Zhu MF, Liu XL, Zhang W, Sun B, Chen YM, Adler HP (2006) High clay content nanocomposite hydrogels with surprising mechanical strength and interesting deswelling kinetics. Polymer 47:1–5

Majdan M, Pikus S, Rzączyńska Z, Iwan M, Maryuk O, Kwiatkowski R, Skrzypek H (2006) Characteristics of chabazite modified by hexadecyltrimethylammonium bromide and of its affinity toward chromates. J Mol Struct 791:53–60

Manilo M, Lebovka N, Barany S (2015) Electrokinetic study of impact of laponite platelets on stabilization of carbon nanotubes in aqueous suspensions. Mater Sci Eng 40:96–104

Molina M, Giulbudagian M, Calder M (2014) Positively charged thermoresponsive nanogels for anticancer drug delivery. Macromol Chem Phys 215:2414–2419

Okay O, Oppermann W (2007) Polyacrylamide–clay nanocomposite hydrogels: rheological and light scattering characterization. Macromolecules 40:3378–3387

Samchenko YuM, Dolyns′kyy HA, Pasmurtseva NO, Poltorats′ka TP, Ul′berh ZR, Hamaliya MF (2015) Hydrogel nanocomposites for thermoinitiated release of photosensitizers. Naukovi zapysky NaUKMA: Khimichni nauky i tekhnolohiyi 170:34–39 **[in Ukrainian]**

Schild HG (1996) Thermal decomposition of PNIPAAM: TGA-FTIR analysis. J Polym Sci Part A Polym Chem 34:2259–2262

Shah N, Patel R (2014) Formulation and development of hydrogel for poly acrylamide-co-acrylic acid. JPSBR 4:114–120

Shibayama M, Suda J, Karino T, Okabe S, Takehisa T, Haraguchi K (2004) Structure and dynamics of poly(NIPAA)–clay nanocomposite gels. Macromolecules 37:9606–9612

Shliomis MI (1974) Magnetic fluids. Uspekhi fizicheskikh nauk 112:427–458 **[in Russian]**

Spizzirri UG, Altimari I, Puoci F (2011) Innovative antioxidant thermo-responsive hydrogels by radical grafting of catechin on inulin chain. Polym J 84:517–523

Steinhilber D, Rossow T, Wedepohl S, Paulus F, Haag R (2013) Biocompatible functionalized polyglycerol microgels with cell penetrating properties. Chem Int Ed 52:13538–13543

Teotia AK, Sami H, Kumar A (2015) Thermo-responsive polymers: structure and design of smart materials. In: Switchable and responsive surfaces and materials for biomedical applications, 1, pp 3–43. https://doi.org/10.1016/b9780857097132.00001-8

Van Vlerken L, Amiji M (2006) Multi-functional polymeric nanoparticles for tumour-targeted drug delivery. Expert Opin Drug Deliv 58:3–205

Wang Y, Chen DJ (2012) Preparation and characterization of a novel stimuli-responsive nanocomposite hydrogel with improved mechanical properties. J Colloid Interface Sci 372:245–251

Xianjing Z, Yuanyuan Z, Jingjing N, Zhichao J, Junting X, Xinghong Z, Binyang D (2014) Thermosensitive ionic microgels via surfactant-free emulsion copolymerization and in situ quaternization cross-linking. Appl Mater Interfaces 6:4498–4513

Xiong LJ, Hu XB, Liu XX, Tong Z (2008) Network chain density and relaxation of in situ synthesized polyacrylamide/hectorite clay nanocomposite hydrogels with ultra-high tensibility. Polymer 49:5064–5071

Yariv S (2004) The role of charcoal on DTA curves of organo-clay complexes: an overview. Appl Clay Sci 24:225–236

Zha L, Banikand B, Alexis F (2011) Stimulus responsive nanogels for drug delivery. Soft Matter 7:5908–5916